

Impact of Extragalactic Sources on Galactic Stellar Trajectories

Bachelor-Arbeit

zur Erlangung des Grades

Bachelor of Science (B.Sc.) im Studiengang Physik

am Department Physik der
Friedrich-Alexander-Universität Erlangen-Nürnberg

vorgelegt am 14. Oktober 2013

von **Marco Fink**



Betreuer: Prof. Dr. Ulrich Heber & Dipl. Phys. Andreas Irrgang

Contents

1	Introduction	1
2	Basics of Galactic Astronomy	3
2.1	Structure of the Milky Way	3
2.2	The Local Group	4
3	The Orbit Calculator	6
3.1	Equations of motion	6
3.2	Constituents of the gravitational potential	8
4	Possible Improvements and Feasibility	10
4.1	Supermassive black hole	11
4.2	The Andromeda galaxy	12
4.3	The Large Magellanic Cloud	13
5	Addition of the Large Magellanic Cloud (LMC)	14
5.1	The LMC potential	14
5.2	Implementation	17
6	Consistency Checks	19
6.1	Stellar orbits inside the LMC	19
6.2	Escape velocity from the LMC	20
7	Consequences	22
7.1	Impact on Galactic disk orbits	22
7.2	Impact on Galactic halo orbits	23
7.3	Tidal disruption of LMC star orbits	24
7.4	Revision of HVS 3	25
8	Conclusion	28

Abstract

Stellar kinematics are an important tool to characterize the stellar populations of the Galaxy. We focus on Galactic halo stars. In order to analyze astrometric measurements and derive Galactic orbits of the stars, the gravitational potential, in particular that of the dark matter halo, needs to be specified. In fact the most extreme halo stars allow us to put stringent constraints on the halo mass. The fastest moving stars, the so-called hypervelocity stars (HVSs), may even exceed the Galactic escape velocity. We use an Orbit Calculator to search for the place of origin of the HVSs. The Orbit Calculator used is a numerical simulation for calculating stellar orbits in a simple model potential of the Milky Way. Three different representations of the dark matter halo are implemented (Irrgang et al., 2013).

Several possibilities on how to improve the gravitational potential are considered, and finally a way to include moving satellite galaxies is developed. As an example, the gravitational potential and motion of the Large Magellanic Cloud (LMC) is implemented and the consequences for the trajectories of halo stars and especially the closely passing B-type star HE 0437-5439 (HVS3) are discussed.

It is found, that from cinematic considerations alone the trajectory of HVS3 can not be confined to the Galactic center as claimed by Brown et al. (2010) and that an origin in the LMC which is also supported by HVS3's lifetime and abundances can not be excluded.

1 Introduction

To calculate past and future stellar trajectories through the Milky Way from observationally determined parameters (distance, coordinates, radial velocity and proper motion), the Remeis Observatory Bamberg uses a scripted simulation written by Lucas Schiefelbein and Andreas Irrgang. In this thesis it will be referred to as „Orbit Calculator”. In the past it was mainly used by the stellar astronomy group to study the kinematics of various classes of stars with the presently most interesting application being the phenomenon of hyper-velocity stars (abbreviated as HVSs), a rare type of halo stars that do not fit to the velocity distribution of their neighborhood but move at such high velocities that they even exceed the galactic escape velocity. Precise calculation of these stars’ trajectories is needed to find the origin and cause of this anomalous behaviour.

One common hypothesis is that the stars are ejected from the Galactic center via the Hills-mechanism (Hills, 1988). According to Hills, the star is ejected by an encounter of a binary (or multiple) star system with the central supermassive black hole. Through multi-body interactions, one of the stars is captured in a close orbit around the black hole while its momentum is transferred to the second star which is ejected at high velocity. But as the uncertainties in proper motion and distance measurements are very high, evidence for this hypothesis is hard to achieve and other origins can not be ruled out. Proper motions are determined from position measurements at different times, but because of the very slow apparent movement of stars, time intervals of at least several years are required to get a measurable change of position. Distances are hard to determine because on these far Galactic scales parallax measurements are not possible, so distances have to be calculated from absolute and apparent magnitude. The absolute magnitude can be derived from the spectral class, but in this case with a large ambiguity: The HVSs discovered by now are mainly late B-type stars, giving the possibility of either a massive young main-sequence star or an old, low-mass horizontal-branch star. Both possibilities lead to very different magnitudes and thus distances. However, the problem can be mitigated somewhat by examining metallicity and rotation velocity (Heber et al., 2008).

Nevertheless HVSs are a promising opportunity for the whole field of Galactic dynamics, as they may be an effective instrument for determining the mass of the dark matter halo of the Galaxy and for probing the potential and thus the mass distribution of the entire Milky Way.

The goal of this Bachelor’s thesis is to improve the original Orbit Calculator which was specially designed to be easy to modify and to add more details to the simplistic, statically modelled Galaxy potential. Therefore I will first

discuss the Orbit Calculator as it exists now and make suggestions on how to refine the model. As will be shown, the satellite galaxies of the Milky Way have the strongest impact on stellar dynamics, with the Large Magellanic Cloud (LMC) as the most dominant one, which I will also implement, check the implementation for consistency and discuss the consequences.

This includes a comparison to the work of Brown et al. (2010). on the origin of HVS 3. The discovery of the star HE 0437-5439 being a hyper velocity star (named HVS 3) has led to some controversy. Location and velocity vector of the star implicate that it is moving on a trajectory that is passing very close to the LMC. The fact that as a spectral type B-star its travelling time from the Galactic center largely exceeds its main-sequence lifetime inspired the idea that its origin could lie within the LMC which would require new mechanisms to accelerate HVSs (Przybilla et al., 2008). However, Brown et al. claim that they can rule out the LMC origin and confirm an ejection from the Galactic center using proper motion data acquired with the Hubble Space Telescope and using a simulation that includes the gravity field of the LMC. As until now this was not possible using the Orbit Calculator the final goal will be to apply the LMC implementation on this problem and to check these results.

2 Basics of Galactic Astronomy

2.1 Structure of the Milky Way

The Milky Way is assumed to be a spiral galaxy similar to many other observed galaxies. Despite its seemingly complex structure, the Milky Way can be described by several easy to grasp components, which are:

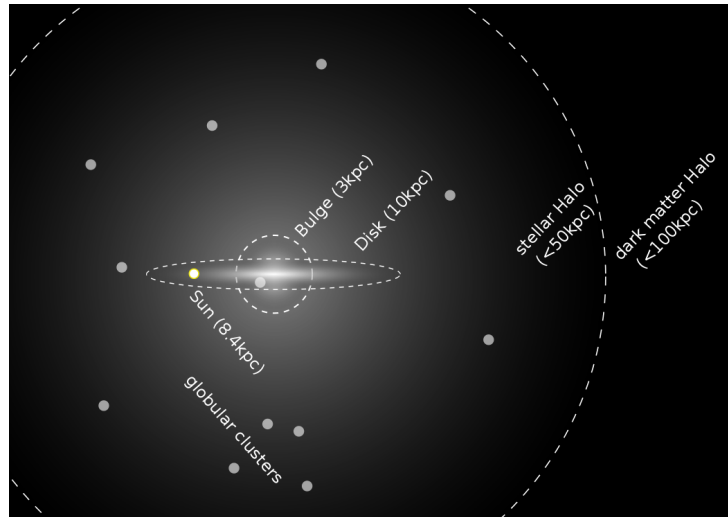


Figure 1: edge-on view of the Milky Way (schematic)

- **The bulge:** A large cluster of older population stars at the center of the Galaxy that contains about 15% of its luminous matter. The velocity vectors of its stars are randomly and spherically distributed at root-mean-square-velocities of $\simeq 150 \text{ km s}^{-1}$. More recent research suggests that the bulge is not exactly spherical, but distorted into an ellipsoidal bar extending up to 3 kpc from the center. At its center, the Bulge hosts the supermassive black hole Sgr A* of $4 \times 10^6 M_{\odot}$ (Binney & Tremaine, 2008).
- **The disk:** The main part of the luminous matter is contained by the disk, consisting of interstellar gas, old and young stars as most of the star formation takes place in the disk, especially in the spiral arms. The central plane of the Galactic disk is generally used as fundamental plane for Galactic coordinate systems. Commonly, star densities inside the disk are modelled to decrease exponentially with distance from the disk plane. The stars of the disk are moving in approximately circular orbits at velocities of $240 \pm 20 \text{ km s}^{-1}$. The sun is located about 8.4 kpc from the Galactic Center, while the Disk extends up to 10 kpc.

- **The stellar halo:** Bulge and disk are surrounded by a large halo of randomly distributed globular clusters and old stars from the Milky Way's first star population. Its contribution to mass and luminosity is negligible, but it extends to 50 kpc from the Galactic center.
- **The dark matter halo:** The observed movements of disk stars, halo stars and clusters do not fit to the mass distribution that is inferred from the luminous objects of the Galaxy. Thus it is assumed that the Milky Way is embedded in a large spherical halo of matter that only interacts by gravity. It makes up 95% of the total mass of the Milky Way and extends to over 100 kpc, strongly shaping the gravitational potential of the Galaxy.
Possible candidates are massive compact halo objects (MACHOs), astronomical objects that emit very little or no light like black holes, cold white dwarfs and neutron stars, or weakly interacting massive particles (WIMPs), assumed but not yet detected elementary particles left over from the Big Bang. Because of the implausible high number of MACHOs required to explain the halo, the second theory is generally preferred.

2.2 The Local Group

In the course of this Bachelor's thesis not only the Milky Way itself, but also its close extragalactic neighbourhood, the so called Local Group will be of interest, which contains:

- **The Large and Small Magellanic Clouds:** The LMC is the galaxy with the largest apparent magnitude due to its small distance of only 45-50 kpc from the Sun. For comparability, we will use the mass assumed by Brown et al. (2010) of $2 \times 10^{10} M_{\odot}$ for the whole LMC, including its possible own dark matter halo, being only 1/50th as massive as the Milky Way.
The Small Magellanic Cloud is much less prominent, but still observable to the naked eye. Both are circling the Milky Way inside its dark halo and are believed to have been a binary galaxy captured and disrupted by the Milky Way. Both are trailed by the Magellanic Stream, an extended band of neutral hydrogen (HI) spanning half the sky. It was most likely ripped out of the Magellanic Clouds by tidal forces of the Milky Way.
- **Satellite Galaxies of the Milky Way:** The Milky Way hosts a whole zoo of other dwarf galaxies orbiting the Milky Way at the outer rim and outside of the halo with the LMC and SMC being just the most conspicuous ones. Other large members of this group are the

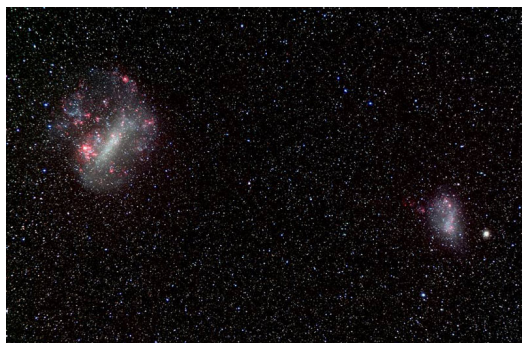


Figure 2: Wide angle photo of the Large and Small Magellanic Clouds
 Source: <http://www.stsci.edu/~inr/thisweek1/2009>

Sagittarius Dwarf and the Canis Major Dwarf of sizes similar to the SMC.

- **The Andromeda and Triangulum Galaxy:** The two closest independent spiral galaxies of sizes comparable to our Milky Way are the Andromeda Galaxy (M31) at about 780kpc and the Triangulum Galaxy (M33) at 850kpc distance. The Andromeda Galaxy is of special interest here, as its high radial velocity of 121 km s^{-1} (SIMBAD) implies a course that leads to a future collision or at least strong gravitational interactions with the Milky Way on a timescale of about 5 billion years.

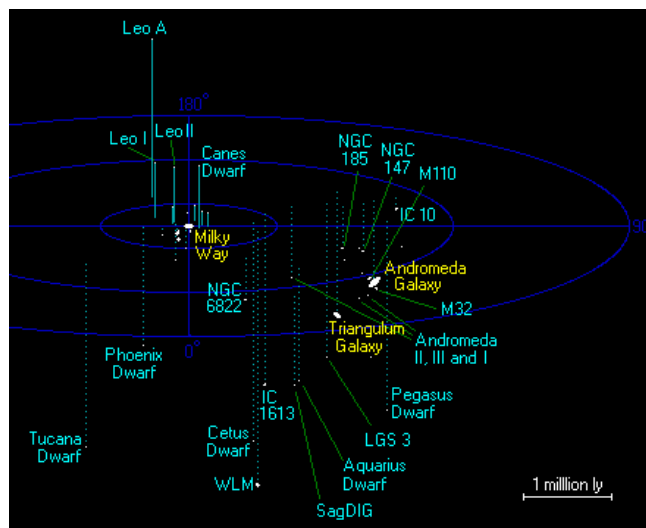


Figure 3: map of the most important members of the local group
 Source: <http://www.atlasoftheuniverse.com/localgr.html>

3 The Orbit Calculator

The Orbit Calculator was written as a script for the astronomically oriented data analysis software ISIS (Interactive Spectral Interpretation System). ISIS uses the scripting language S-Lang which is based on C.

The Calculator is an extended S-Lang function that takes coordinates and velocities for a particle and an end time as arguments, as well as several qualifiers that activate specific options or change internal parameters of the simulation. It returns fields containing the initial and final coordinates and velocities, optionally the calculated points for the whole trajectory can be saved.

Input coordinates can be in either celestial or Galactocentric Cartesian coordinates, internally the computations are handled in Galactic cylindrical coordinates which will also be used in the following for the sake of simplicity.

Physical values will be expressed in units of km s^{-1} for velocity, kpc for distances and masses in galactic mass units of $M_{\text{gal}} = 2.325 \times 10^7 M_{\odot}$ introduced by Allen & Santillan (1991). The galactic mass units are defined so that the gravitational constant G appearing in the potential expressions turns 1 when expressing velocities in km s^{-1} and lengths in kpc.

3.1 Equations of motion

At its mathematical core, the Orbit Calculator treats a single particle moving through an axisymmetric gravitational potential. The according equations of motion are derived using the Lagrange formalism. The Lagrangian in classical mechanics is easily calculated from kinetic energy E and potential energy U . To make use of the axisymmetry, the problem is expressed in cylindrical coordinates.

$$L(r, \phi, z, \dot{r}, \dot{\phi}, \dot{z}) = E - U = \frac{1}{2} \left(\dot{r}^2 + (r\dot{\phi})^2 + \dot{z}^2 \right) - \Phi(r, \phi, z)$$

The corresponding canonical momenta $p_i = \frac{\partial L}{\partial \dot{q}_i}$ are:

- $p_r = \dot{r}$
- $p_{\phi} = r^2 \dot{\phi}$; further referred to as angular momentum L_z .
- $p_z = \dot{z}$

Using these, the Lagrange equations $\frac{d}{dt} \frac{\partial L}{\partial \dot{q}_i} = \frac{\partial L}{\partial q_i}$ are evaluated:

- $\dot{p}_r = r\dot{\phi}^2 + \frac{\partial \Phi}{\partial r} = \frac{p_\phi^2}{r^3} + \frac{\partial \Phi}{\partial r}$
- $\dot{p}_\phi = \frac{\partial \Phi}{\partial \phi}$
- $\dot{p}_z = \frac{\partial \Phi}{\partial z}$

These equations of motion can be solved numerically if the potential function with arguments of r, z, ϕ is known.

3.2 Constituents of the gravitational potential

The potential function Φ consists of several additive components that correspond to the structure of the Milky Way as explained in section 2.1 – bulge, disk and dark matter halo. The stellar halo is not massive enough to have a notable contribution and is thus neglected.

$$\Phi(r, z) = \Phi_{bulge} + \Phi_{disk} + \Phi_{halo} \quad (1)$$

Owing to superposition of forces, any further corrections to the potential can simply be added as additional term to the potential sum. The current implementation consists of the following terms:

- **Bulge:**

$$\Phi_{bulge}(r, z) = -\frac{M_b}{\sqrt{r^2 + z^2 + b_b^2}} \quad (2)$$

with mass M_b and scale length b_b of the bulge. This potential function was originally introduced by Plummer in 1911 for the description of globular clusters. For large distances, it converges against the $\frac{1}{r}$ -potential of a point mass while delivering a forceless minimum at its center.

- **Disk:**

$$\Phi_{disk}(r, z) = -\frac{M_d}{\sqrt{r^2 + (a_d + \sqrt{z^2 + b_d^2})^2}} \quad (3)$$

with Mass M_d and two scale lengths a_d, b_d of the disk. A modified version of the Plummer-potential, which is compressed along the z -axis, delivering axisymmetric ellipsoids for equipotential surfaces.

- **Dark Halo:**

for $R < \Lambda$, where $R = \sqrt{r^2 + z^2}$:

$$\Phi_{halo}(R(r, z)) = \frac{M_h}{a_h} \left(\frac{1}{(\gamma - 1)} \ln \left(\frac{1 + \left(\frac{R}{a_h}\right)^{\gamma-1}}{1 + \left(\frac{\Lambda}{a_h}\right)^{\gamma-1}} \right) - \frac{\left(\frac{\Lambda}{a_h}\right)^{\gamma-1}}{1 + \left(\frac{\Lambda}{a_h}\right)^{\gamma-1}} \right) \quad (4)$$

otherwise:

$$\Phi_{halo}(R(r, z)) = -\frac{M_h}{R} \frac{\left(\frac{\Lambda}{a_h}\right)^\gamma}{1 + \left(\frac{\Lambda}{a_h}\right)^{\gamma-1}} \quad (5)$$

This is the first of three different implemented dark halos, originally used by Allen & Santillan (1991). For the sake of simplicity, the simulations presented in this work will stick to this single halo potential. Out of the three halos, Allen & Santillan's delivers a well-fitting rotation curve but includes a singularity at $R = 0$ and requires a cut-off Λ at large radii to prevent the integrated mass from getting infinite. In practice, the cut-off happens at $R = 200$ kpc and thus doesn't affect the stellar trajectories that lie well within this range.

The other two halo models are those proposed by Wilkinson & Evans (1999) and Navarro et al. (1997). The Wilkinson & Evans halo gives a finite mass, but its rotation curve falls off rapidly at large distances. The Navarro-Frenk-White potential is the only potential that is theoretically grounded as it was derived from cosmologic N-body simulations modelling the clustering of dark matter. However, its rotation curve rises for large distances and the total mass deviates strongly from the aforementioned.

The whole process of achieving the three halos' parameters is explained in detail in the publication of Irrgang et al. (2013).

As none of these potentials depends on ϕ due to axial symmetry, the second Lagrange equation $\dot{p}_\phi = \dot{L}_z = \frac{\partial \Phi}{\partial \phi}$ equals zero, representing the conservation of angular momentum:

$$\frac{dL_z}{dt} = 0 \implies L_z = \text{const.}$$

This can be exploited in the numerical calculation so that only five instead of six coupled differential equations have to be solved.

4 Possible Improvements and Feasibility

To make the simulation more realistic, the most massive structures that were not already included in the above are analyzed for the size and strength of their gravitational influence and for the possibility of an implementation.

As a criterion for the impact of the new gravitational source on star trajectories, the forces exerted by the Milky Way and by the additional source are compared at every point of a plane through the Galactic center. Therefore, the fraction i of the additional force F_{new} divided by the Milky Way's force F_{MW} is evaluated and illustrated as heat-map.

$$i = \frac{|F_{new}|}{|F_{MW}|}$$

The Milky Ways force is derived from the bulge and disk potentials shown in section 3.2 while for these considerations the much simpler halo potential from Wilkinson & Evans (1999) is used as it is easier to handle analytically.

$$\Phi_{halo}(R) = -\frac{M_h}{a_h} \ln \left(\frac{\sqrt{R^2 + a_h^2} + a_h}{R} \right)$$

Also, the disks potential is approximated as spherical using a mean value of the two scale parameters. The candidates for additional sources are represented by point-masses and respectively a Plummer potential. The used parameters are displayed in the following table:

source	scale parameter (kpc)	mass (M_{Gal})	
bulge	0.2	200	
disk	2.5	2800	spherical approx.
halo	200	69725	
Sgr A*	–	0.2	point-mass
M31	–	70000	point-mass
LMC	1.0	860	

It is assumed that the added source only has a significant impact on trajectories where its force surpasses 5% of the Galactic force, marked as yellow area in the colour plot.

4.1 Supermassive black hole

First, the supermassive black hole Sagittarius A* at the center of the Galaxy is considered. As a point-mass of $0.2 M_{\text{Gal}}$ at the origin of the simulation it would be easily implemented in analogy to the already existing components.

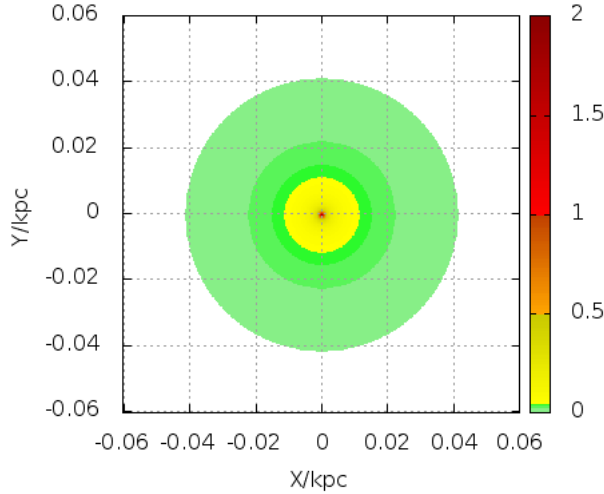


Figure 4: inside the green circle, the force exerted by Sgr A* reaches 1% of the Milky Way's, inside the yellow circle it surpasses 5%. Bearing in mind the axis scaling, the black hole contributes significantly to the Galactic force field only in the innermost 10pc.

The colour plot 4 shows, that Sgr A* is only of interest in the very central parsecs of the Galaxy, but here the modelling of the Orbit Calculator leads to some problems. The Galactic dark matter halo potential by Allen & Santillan contains a physically not very reasonable singularity at the center making the simulation unreliable in the inner parsecs. And when tracing back a star trajectory from the Galactic halo, the propagated high uncertainties of the stellar motion will make it unlikely that the stars trajectory can be confined to the small area where the black hole would be of significance.

4.2 The Andromeda galaxy

The Andromeda galaxy is assumed about the same mass as the Milky Way and placed at a distance of 780 kpc. The large distance would justify a simple implementation as a point-mass set off from the center, thus being only slightly more complicated than an implementation of Sgr A*.

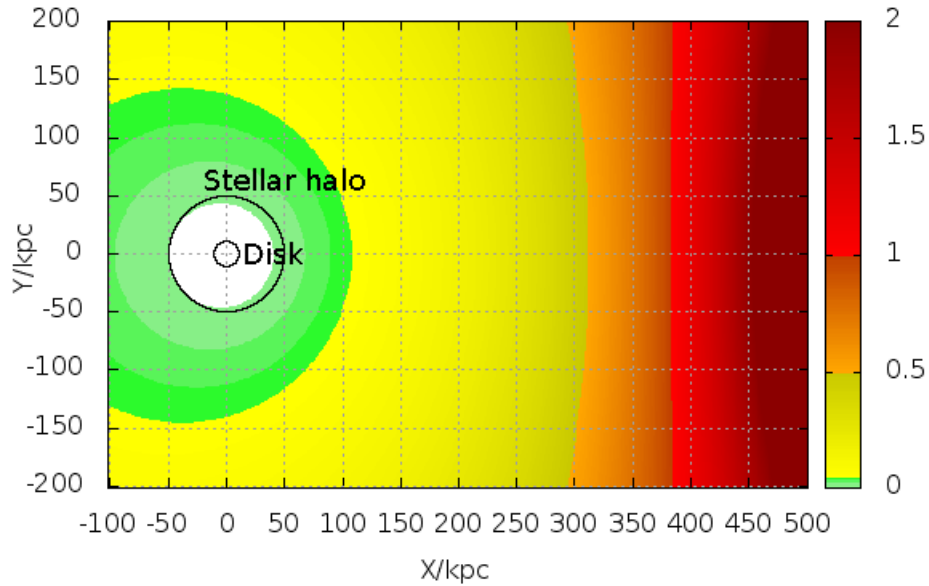


Figure 5: The plotted plane goes through the centers of the Milky Way and the Andromeda galaxy which lies outside of the plot at $x = 780$ kpc, $y = 0$. Assuming the two galaxies' potentials to be spherically symmetric by neglecting the disk components, the whole information can be shown in a 2-dimensional plot. The extent of the Galactic disk and halo are marked as black circles. The force of M31 reaches 5% of that of the Milky Way in the yellow area, 50% in the orange area and begins to dominate in the red area.

As figure 5 illustrates, M31 has to be accounted for only at distances over 100 kpc from the Galactic center, far from the main part of the stellar halo population. The Triangulum galaxy, being slightly farther away and less massive would be even less important.

4.3 The Large Magellanic Cloud

The LMC is currently located about 50 kpc from the Galactic center, however it is moving on the same timescales as the other halo stars, with this distance strongly varying. Thus its movement would have to be accounted for, making an implementation more complex than the above candidates.

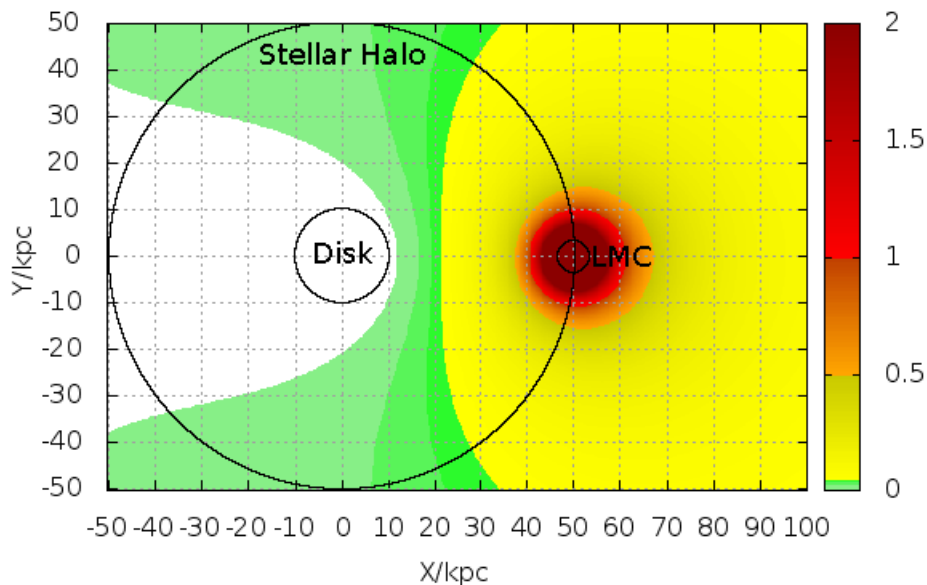


Figure 6: As in figure 5 both galaxies are approximated as spherical with the drawn x-axis through both galaxies' centers. The extents of their disks are marked by black circles. The yellow area of 5%-significance reaches well within the stellar halo. The red area, where the LMC's force outweighs the Galaxy's, is where orbits are bound to the LMC.

Figure 6 shows that all trajectories within at least 30 kpc of the LMC are significantly influenced, and that even a large part of the LMC's potential well lies within the Galactic Halo. Considering this the implementation of the LMC will be the most rewarding, also as the developed model can afterwards easily be adopted for other satellite galaxies or globular clusters.

5 Addition of the Large Magellanic Cloud (LMC)

As discussed before, the most feasible improvement is the inclusion of satellite galaxies in the potential. A method to include moving satellite galaxies is developed and implemented using data of the LMC.

5.1 The LMC potential

Because of the small extent of the LMC compared to the Milky Way's potential, it would be sufficient to approximate the LMC's potential as moving point mass. However, to prevent a singularity, it is more feasible and also realistic to reuse the Plummer-model already used for the bulge. It approaches the point-mass potential fast enough for distances larger than the extent of the LMC of about 3 kpc while yielding a flat minimum at the center (compare figure 7). Still this is a very rough model. The LMC is known to show disk and spiral features, and also to possess its own dark matter halo. But as for these features reliable data are not available, and as they can be neglected outside the LMC itself, the simpler model of a spherically symmetric mass distribution, including luminous and dark matter in one potential function, is used here.

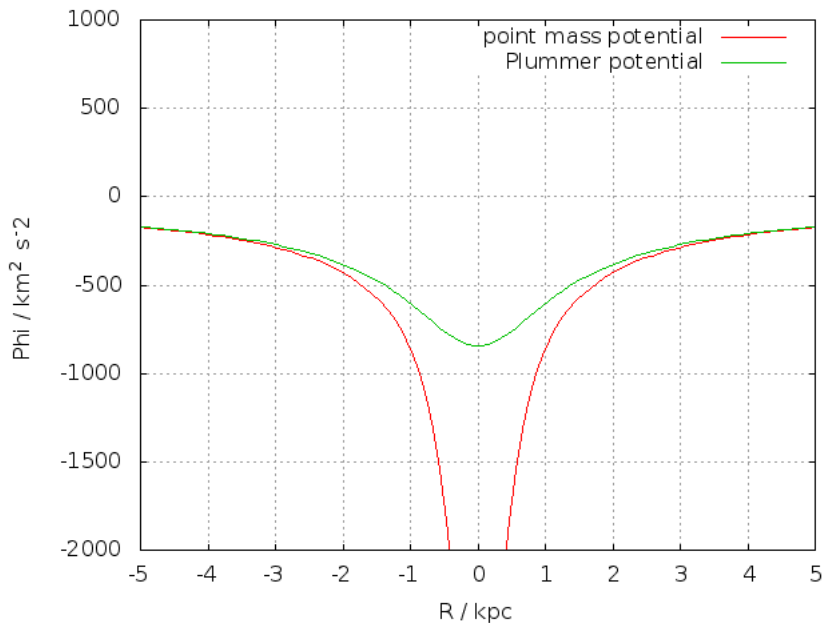


Figure 7: Plummer and point mass potential using the parameters of the Large Magellanic Cloud derived in the following paragraph

Determining potential parameters

To complete the Potential, the Mass M_{LMC} and scale parameter b_{LMC} are required. For later comparability we will use the data also used by Brown et al. (2010) for their calculation of HVS3's trajectory, assuming a mass of $M_{LMC} \simeq 2 \times 10^{10} M_{\odot}$ with 85% of the LMC's mass inside of a radius of 3 kpc. To relate the potential function to the respective mass distribution, we use the Poisson-equation

$$\Delta\Phi(R) = 4\pi\rho(R)$$

Evaluated for the Plummer potential $\Phi(R) = -\frac{M}{\sqrt{R^2+b}}$ it gives the density distribution

$$\rho(R) = \frac{3b^2M}{4\pi(R^2 + b^2)^{\frac{5}{2}}} \quad (6)$$

Now the assumption is used that 85% of the LMC's mass are found inside 3 kpc. The right side is obtained by integrating the density distribution over a sphere of 3 kpc radius.

$$0.85M_{LMC} = M_{3kpc} = \int_0^{3kpc} 4\pi R^2 \rho(R) dR \quad (7)$$

The evaluated integral yields:

$$0.85M_{LMC} = \int_0^{3kpc} \frac{3R^2 b^2 M_{LMC}}{(R^2 + b^2)^{\frac{5}{2}}} dR = \left[\frac{M_{LMC} R^3}{(R^2 + b^2)^{\frac{3}{2}}} \right]_0^{3kpc} \quad (8)$$

Inserting integration limits and solving for b gives:

$$b = 0.33828 \cdot 3kpc = 1.0148kpc$$

So the shape of the LMC's potential is fully defined.

The moving LMC

With the shape of the potential determined, it is now set to the correct position. Therefore, we begin with the Plummer function in Cartesian coordinates.

$$\Phi_{LMC}(x, y, z) = -\frac{M_{LMC}}{\sqrt{x^2 + y^2 + z^2 + b^2}} \quad (9)$$

This function is now shifted by the LMC's current (Cartesian) coordinates x_{LMC} , y_{LMC} , z_{LMC} giving

$$\Phi_{LMC}(x, y, z) = -\frac{M_{LMC}}{\sqrt{(x - x_{LMC})^2 + (y - y_{LMC})^2 + (z - z_{LMC})^2 + b^2}}$$

The coordinates x , y and z are now expressed in cylindrical coordinates, as required for the differential equation solver of the Orbit Calculator.

- $x(r, \phi) \longrightarrow r \cdot \cos(\phi)$
- $y(r, \phi) \longrightarrow r \cdot \sin(\phi)$
- $z \longrightarrow z$

so that

$$\Phi_{LMC}(r, z, \phi) = -\frac{M_{LMC}}{\sqrt{(r \cos(\phi) - x_{LMC})^2 + (r \sin(\phi) - y_{LMC})^2 + (z - z_{LMC})^2 + b^2}}$$

To move the LMC potential, the coordinates of the LMC's center x_{LMC} , y_{LMC} , z_{LMC} are simply replaced by the time dependent coordinates $x_{LMC}(t)$, $y_{LMC}(t)$, $z_{LMC}(t)$. These are computed using the Orbit Calculator itself after calling up on starting coordinates and velocity of today's LMC.

Adding this to the existing potential the complete new potential function is:

$$\Phi(r, z, \phi, t) = \Phi_{bulge}(r, z) + \Phi_{disk}(r, z) + \Phi_{halo}(r, z) + \Phi_{LMC}(r, z, \phi, t)$$

5.2 Implementation

The model described in section 5.1 is now concretely implemented in the numerical simulation. For the exact lines of ISIS-code that were added, see the appendix.

Calculation of the LMC's trajectory

Upon loading of the script, the trajectory of the LMC is calculated using the Orbit Calculator and the standard model with the Allen & Santillan-potential. The calculation uses celestial coordinates, proper motion and radial velocities from SIMBAD and the same distance as Brown et al. (2010). Two trajectories are calculated each 5000 Myrs into the past and future and stored in the two arrays *lmcn.tr.o0* and *lmc.p.tr.o0* for positive and negative time values.

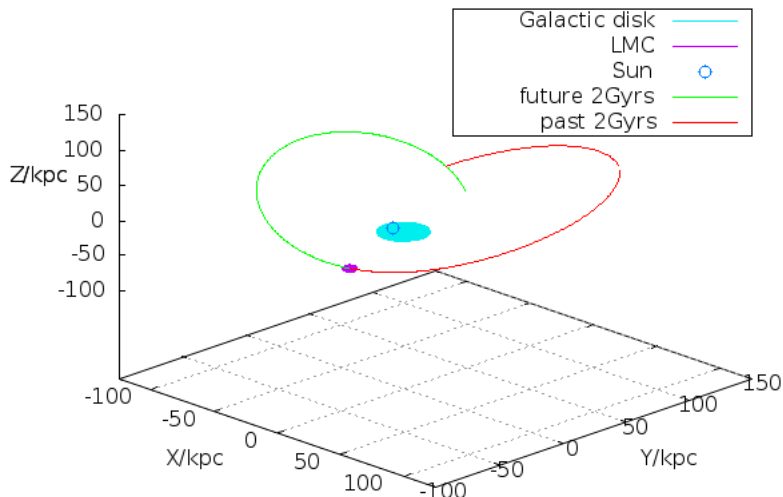


Figure 8: One orbit of the simulated LMC spanning 2Gyrs each into past and future

Interpolation of LMC positions from the trajectory array

As the differential equation solver adaptively determines the length of time steps to keep errors low, the time steps of later trajectory simulations generally do not match those of the LMC's trajectory. Thus a function is defined to determine the position of the LMC at any time. As argument, it takes any time value between -5000 and 5000 Myrs and returns the according

Cartesian coordinates x_{LMC} , y_{LMC} , z_{LMC} of the LMC. The values are interpolated linearly from the LMC trajectory arrays *lmcn.tr.o0* and *lmc.p.tr.o0* using ISIS's own interpolation function.

Equations of motion

Finally, the equations of motion presented in 3.1 are supplemented by the respective LMC terms.

- $\dot{p}_r = \frac{p_\phi^2}{r^3} + \frac{\partial\Phi_{MW}}{\partial r} + \frac{\partial\Phi_{LMC}}{\partial r}$
- $\dot{p}_\phi = \frac{\partial\Phi_{MW}}{\partial\phi} + \frac{\partial\Phi_{LMC}}{\partial\phi}$
- $\dot{p}_z = \frac{\partial\Phi_{MW}}{\partial z} + \frac{\partial\Phi_{LMC}}{\partial z}$

The three partial derivations of the LMC potential in the directions of r , z , and ϕ have to be calculated, delivering the gravitational force exerted by the LMC.

$$\frac{\partial\Phi_{LMC}}{\partial r} = \frac{M_{LMC} (2 \sin \varphi (\sin \varphi r - y_{LMC}) + 2 \cos \varphi (\cos \varphi r - x_{LMC}))}{2 \left((z - z_{LMC})^2 + (\sin \varphi r - y_{LMC})^2 + (\cos \varphi r - x_{LMC})^2 + b^2 \right)^{\frac{3}{2}}}$$

$$\frac{\partial\Phi_{LMC}}{\partial\phi} = \frac{M_{LMC} (2 \cos \varphi r (\sin \varphi r - y_{LMC}) - 2 \sin \varphi r (\cos \varphi r - x_{LMC}))}{2 \left((z - z_{LMC})^2 + (\sin \varphi r - y_{LMC})^2 + (\cos \varphi r - x_{LMC})^2 + b^2 \right)^{\frac{3}{2}}}$$

$$\frac{\partial\Phi_{LMC}}{\partial z} = \frac{M_{LMC} (z - z_{LMC})}{\left((z - z_{LMC})^2 + (\sin \varphi r - y_{LMC})^2 + (\cos \varphi r - x_{LMC})^2 + b^2 \right)^{\frac{3}{2}}}$$

The LMC coordinates x_{LMC} , y_{LMC} , z_{LMC} are calculated at the beginning of every time-step using the aforementioned interpolation function. Obviously, the axial symmetry is broken, represented by the ϕ -derivation being non-zero, and thus the angular momentum is no longer conserved. Together with the now time dependent changes in the potential shape, even the energy of test particles is not conserved, allowing drastic orbit changes through LMC-encounters like capturing and ejections or swing-by maneuvers.

6 Consistency Checks

It is checked whether the numerical simulation produces results that fit the physical model from section 5.

6.1 Stellar orbits inside the LMC

By simulating stars close to the LMC's position and velocity, it is shown that the new potential not only simulates small disturbances on Milky Way orbits, but that also orbits which are bound to the LMC and stable over long times are possible. An example is demonstrated in figure 9.

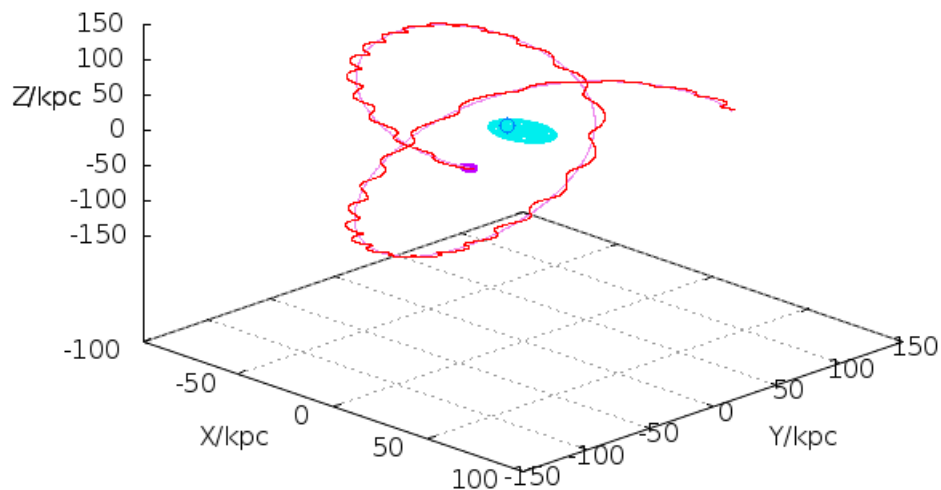


Figure 9: Starting positions and extent of the LMC and the Milky Way are marked by the violet and blue ellipsoids, the LMC trajectory for 5Myrs is shown in violet. The red test star trajectory started with position and velocity close to the LMC's and keeps oscillating around the LMC trajectory during the whole simulation.

6.2 Escape velocity from the LMC

The escape velocity can be easily derived analytically and easily determined from test simulation runs, allowing a simple consistency check.

Mathematically, the escape velocity is simply achieved by identifying the potential energy of the LMC Plummer potential with the kinetic energy of a test particle.

$$E_{pot}(r) = \frac{GMm}{\sqrt{r^2 + b^2}} = \frac{m}{2}v_{esc}^2 \quad (10)$$

solving for v_{esc}

$$v_{esc}(r) = \sqrt{\frac{2GM}{\sqrt{r^2 + b^2}}} \quad (11)$$

and evaluating at $r = 0$ for the parameters M_{LMC} and b_{LMC} gives the escape velocity from the center of the LMC

$$v_{esc}(r = 0) = \sqrt{\frac{2GM_{LMC}}{b_{LMC}}} \simeq 420 \frac{km}{s} \quad (12)$$

this assumes that the Milky Way's potential near the LMC is comparably flat and that centrifugal forces caused by the LMC's motion have no large impact.

For comparison, several test trajectories are evaluated starting at the position of the LMC and with a relative velocity between test star and LMC of zero. The radial velocity of the test star with respect to the Milky Way, and thus also the relative velocity is increased in steps of 10 km s^{-1} until the star is no longer bound. Bound states can easily be distinguished from unbound ones as they are oscillating closely to the LMC's orbit as shown in figure 10.

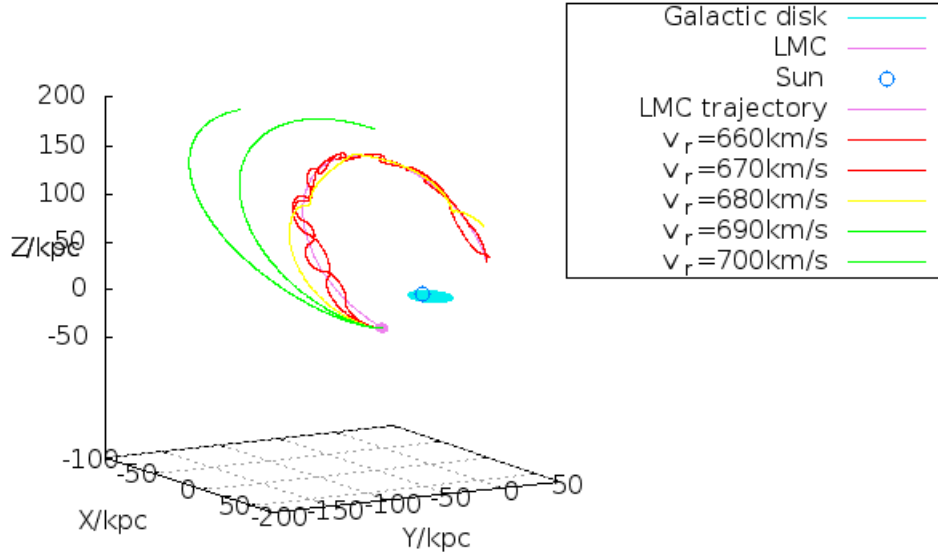


Figure 10: The five test trajectories closest to escape velocity, red orbits are definitely bound to the LMC, oscillating around the violet LMC-orbit, green trajectories are escaping. The yellow orbit is very loosely bound with very long periods, and likely to be disrupted by the Milky Way-LMC-interaction as described in section 7.3

Comparing the trajectories above shows that the yellow one at $v_{rad}=680\text{ km s}^{-1}$ is just close to being unbound while the green one at $v_{rad}=690\text{ km s}^{-1}$ is definitely unbound. As transversal velocities were chosen equal to the LMC's, only the LMC's inherent radial velocity of 283 km s^{-1} has to be subtracted, giving an escape velocity of

$$v_{esc} = 402 \pm 5 \frac{km}{s}$$

Given that in the analytical derivation interactions with the Milky Way potential are completely neglected, the results are convincingly consistent also in a quantitative way.

7 Consequences

With the now implemented LMC potential, the now appearing differences from the earlier Milky Way potential are discussed using some individual example trajectories.

7.1 Impact on Galactic disk orbits

First, some stars in the Galactic disk are calculated and displayed in figure 11.

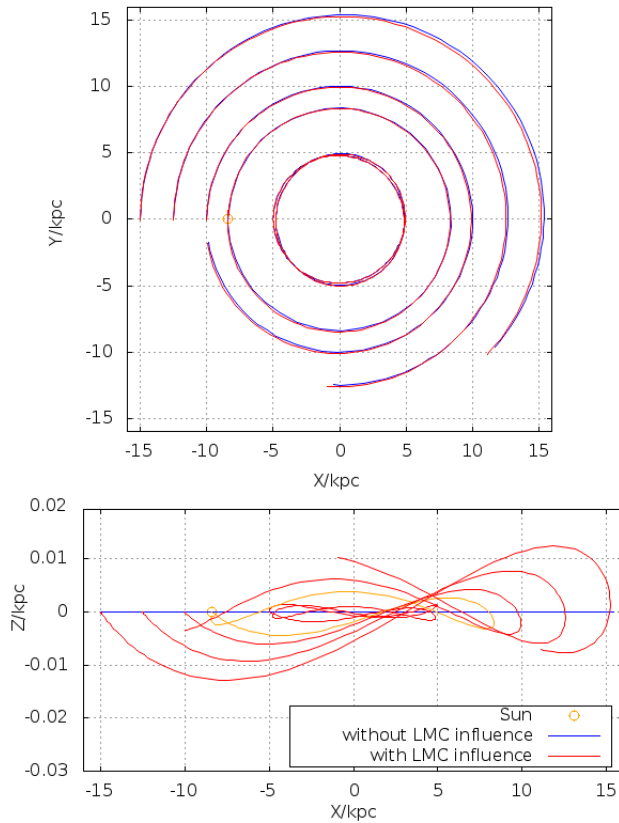


Figure 11: Test stars were started matching the disks rotation curve in steps of 2.5 kpc from the center and at solar distance and calculated for 250 Myrs (period of one solar orbit). Orbits using just the Milky Way potential are coloured blue while orbits accounting also for the LMC potential are coloured red. The Sun's position and orbit are highlighted in orange. The upper image shows the top view of the Galactic disk, the lower one the edge-on view with a greatly exaggerated z-axis.

As expected from the force comparison in graphic 6, the trajectories show no noteworthy deviations whether the LMC is included in calculations or not. On the outermost orbits, changes are noticeable, but in practice largely outweighed by the uncertainties of measurement.

7.2 Impact on Galactic halo orbits

Now orbits on distances representing the Galactic halo are calculated. The considered orbits are circular using velocities on the Galaxy's rotation curve. Although this is not completely realistic for halo orbits, the resulting orbits shown in figure 12 are easier to compare.

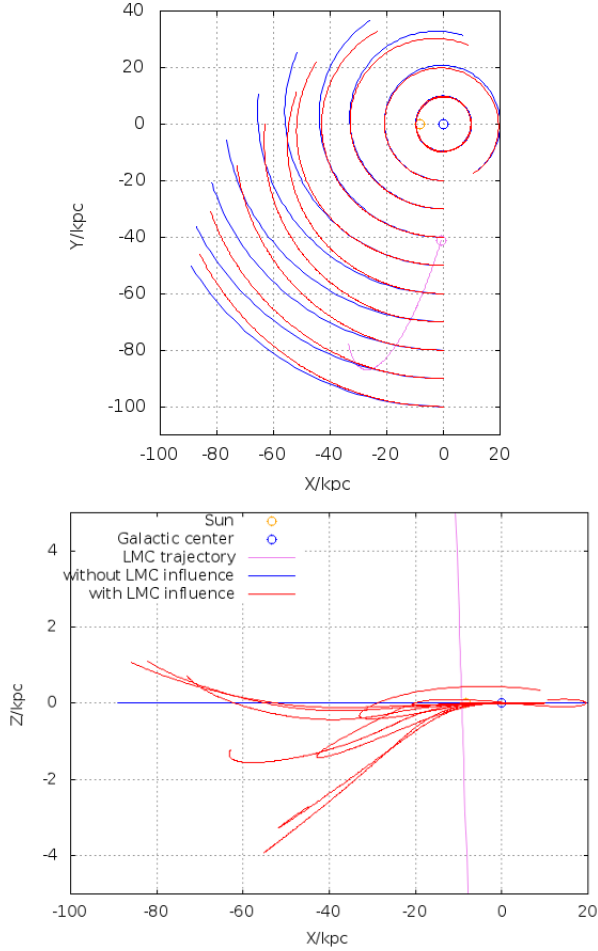


Figure 12: 10 test star orbits in the galactic plane were started in the half-space containing the LMC starting every 10 kpc over a time of 500 Myrs. Standard Milky Way orbits are plotted blue, while LMC influenced orbits are plotted red. The position of the Sun is marked in orange and the Galactic center in blue. The violet LMC trajectory begins below the disk at the marked spot and crosses the disk halfway through the simulation.

All test halo orbits show strong variations with the endpoints deviating by 1 to 10 kpc. The x-z-plot also shows that LMC-assisted orbital plane changes by several degrees happen. This confirms that the implementation of the LMC indeed was justified and that its area of influence lies in the magnitude of order expected from section 4.3.

7.3 Tidal disruption of LMC star orbits

An interesting phenomenon that is now possible is the ejection of stars on an orbit loosely bound to the LMC through the interaction between the two potentials. This example star started 5 kpc from the LMC's center at a relative velocity of 20 km s^{-1} .

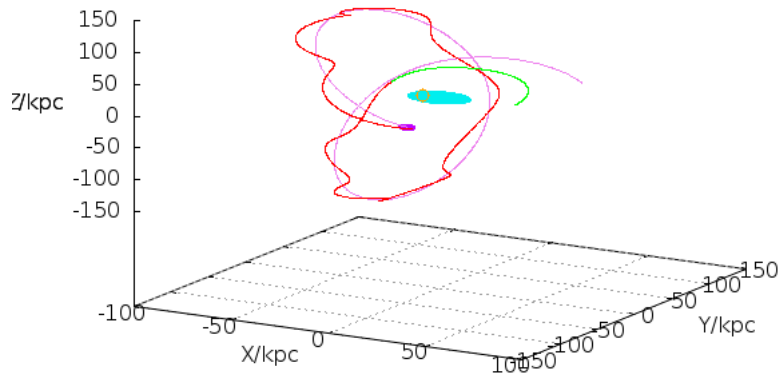


Figure 13: The red test stars orbit is bound to the violet LMC trajectory, until the LMC reaches its perigalacticon where the star leaves the LMC's gravity well and enters a high Milky Way orbit, marked in green.

The resulting star orbit is stable over a whole Milky Way orbit of the LMC, but gets disrupted at the perigalacticon of the LMC orbit. The Star ends on a high elliptical Milky Way orbit with a velocity of 350 km s^{-1} at its perigalacticon of 25 kpc. So this is an example for a possible mechanism for producing stars on the high end of the halo's velocity distribution.

7.4 Revision of HVS 3

As already outlined in the introduction the case of HE 0437-5439 features a serious paradox when adhering to the paradigm of the Hills-ejection. From spectral analysis chemical composition and rotational velocity could be determined to fit that of a main-sequence star. But together with the spectral type B this implies an age of the star between 25 and 35 Myrs. Contradictory, when assuming an ejection from the Galactic center, tracing back possible trajectories gives a flight time of roughly 100 Myrs. This could be resolved by assuming HE 0437-5439 to be a blue straggler – ejected still as binary star from the Galactic center and later on merging to the now observed B-star. The whole configuration would have the required lifetime but with the drawback of the unlikely, but not impossible binary ejection. However, Przybilla et al. (2008) found the elemental abundance pattern to exclude a Galactic bulge origin but being consistent with abundances only found at the edge of the disk and in the much closer LMC.

Therefore HVS3 is an interesting candidate to apply the modified potential. Several trajectories were calculated using the following values:

- coordinates: Ra $4^h 38^m 12.8^s$; Dec $-54^\circ 33' 12''$
- distance d (kpc): 61 ± 9
- proper motion μ_α (mas yr^{-1}): $0.53 \pm 0.25 \pm 0.33$ (stat. and sys.)
- proper motion μ_δ (mas yr^{-1}): $0.09 \pm 0.21 \pm 0.48$
- radial velocity v_{rad} (km s^{-1}): 723 ± 3

To account for the high uncertainties, several trajectories were calculated using proper motions at the edge of the statistical $1\text{-}\sigma$ -interval, giving a cone-like shape of possible trajectories. Both the original and the modified potential were considered in figure 14.

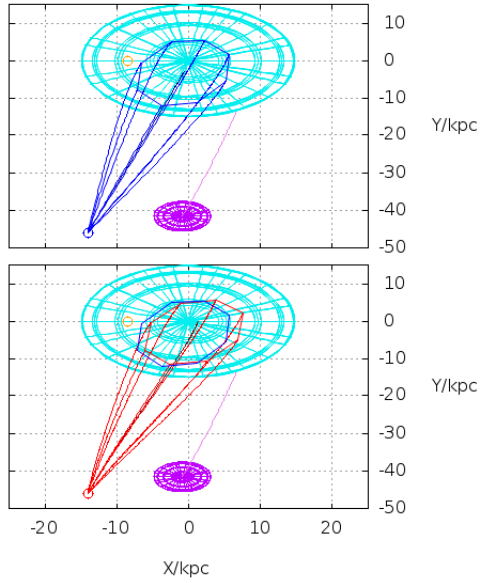


Figure 14: Eight possible trajectories using proper motions at the edge of the $1\text{-}\sigma$ -uncertainty shown in top down view. Current position and extent of the LMC's main population is marked by the purple sphere trailed by its flight path over 100 Myrs. The octagon lies in the Galactic plane where trajectories are cut off because they become unpredictable due to interactions with the interstellar medium. Blue trajectories use the original, red the modified gravitational potential.

Including the LMC slightly increases the size of the $1\text{-}\sigma$ -area, which spans over half the diameter of the Milky Way's disk. Bearing in mind that the distance uncertainties as well as systematic errors in the proper motion components were not even considered, the claim that HVS 3 originated in the Galactic center seems very unstable if it is only supported by trajectory simulations.

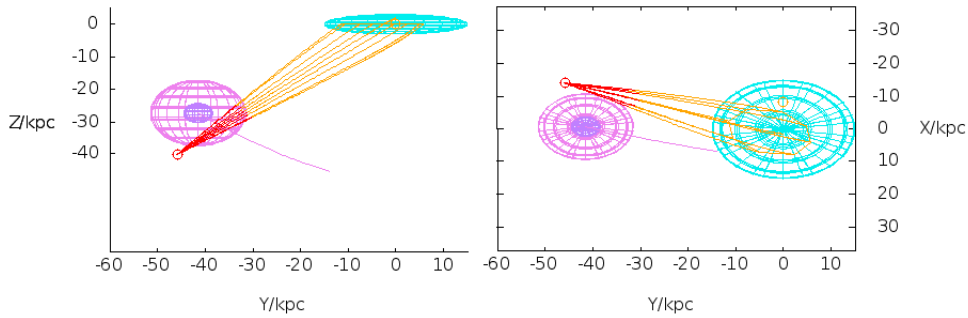


Figure 15: The same problem from two perspectives, HVS3's maximum lifetime of 35 Myrs is highlighted in red. In addition to figure 14 the gravity well of the LMC is marked in violet.

In fact, when also accounting for the distance uncertainty, trajectories out of the LMC's potential well are possible inside the error range like the following example (figure 16) illustrates. It started at $d = 70$ kpc, $\mu_\alpha = 0.71$ and $\mu_\delta = 0.27$ with unchanged right ascension, declination and radial velocity.

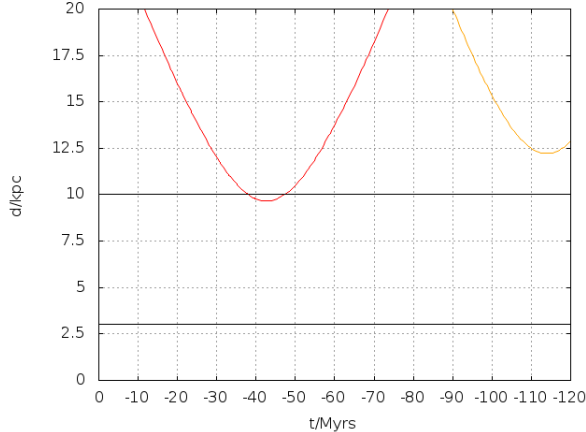


Figure 16: Distance over time from star to LMC in red and to the Galactic center in orange. The extents of the LMC potential well (10 kpc) and the Galactic bulge (3 kpc) are marked black.

Not only does the trajectory lead inside the region where stable LMC-bound orbits are possible, it also passes the Milky Way far from the Galactic bulge. It has also to be kept in mind that mass estimations for the LMC are still subject to change and that there are publications assuming an even larger extent of the LMC like Weinberg & Nikolaev (2001) who find stellar populations and tidal debris of the LMC extending up to 14 kpc. Anyway, trajectories from the center of the LMC seem rather unlikely. But ejection events from a higher LMC orbit caused by other mechanisms than the Hills-scenario lie well within the realm of possibility. Such mechanisms would be the disruption of a binary star by a supernova (Blaauw, 1961) or through multiple body interactions in dense star clusters, perhaps assisted by an intermediate mass black hole as proposed by Gualandris & Portegies Zwart (2007).

8 Conclusion

With the modelling of moving satellite galaxies a simple, but for some cases very important detail has been added to the Orbit Calculator's gravitational potential. The Implementation produces consistent and reliable results and opens up the possibility to be easily expanded on the whole zoo of satellite galaxies orbiting the Milky Way as soon as reliable data on their masses and movements become available. Here the Small Magellanic Cloud would be the next feasible step as it is the next best observed satellite. But if ever a larger number of satellites of similar mass would have to be simulated at once, gravitational reaction between those will play a significant role. Thus the Orbit Calculator would first have to be adapted for treating N-body problems.

The application on HVS3 has shown that the case can definitely not be closed yet. Due to the high uncertainties in proper motion the trajectory's point of origin can not be confined to the Galactic center. Also, neither the Galaxy nor the LMC can be ruled out as place of origin from cinematic considerations alone. Until more reliable motion data are available, the part of the LMC within the margin of error could be examined for clusters large enough to host possible ejection mechanisms.

References

- Allen C., Santillan A., 1991, *Rev. Mexicana Astron. Astrofis.*22, 255
- Binney J., Tremaine S., 2008, *Galactic Dynamics: Second Edition*, Princeton University Press
- Blaauw A., 1961, *Bull. Astron. Inst. Netherlands*15, 265
- Brown W.R., Anderson J., Gnedin O.Y., et al., 2010, *ApJ*719, L23
- Gualandris A., Portegies Zwart S., 2007, *MNRAS*376, L29
- Heber U., Edelmann H., Napiwotzki R., et al., 2008, *A&A*483, L21
- Hills J.G., 1988, *Nature*331, 687
- Irrgang A., Wilcox B., Tucker E., Schiefelbein L., 2013, *A&A*549, A137
- Navarro J.F., Frenk C.S., White S.D.M., 1997, *ApJ*490, 493
- Przybilla N., Nieva M.F., Heber U., et al., 2008, *A&A*480, L37
- Weinberg M.D., Nikolaev S., 2001, *ApJ*548, 712
- Wilkinson M.I., Evans N.W., 1999, *MNRAS*310, 645

Appendix: Code changes

The additions described in section 5 are implemented in the Orbit Calculator through the following lines.

Calculation of the LMC's trajectory

```
variable lmcp = orbit_calculator(05, 23, 34.6, -69, 45, 22, 50,
    283, 1.89, 0.39, 5000; set, model="AS");

variable lmcn = orbit_calculator(05, 23, 34.6, -69, 45, 22, 50,
    283, 1.89, 0.39, -5000; set, model="AS");
```

Upon loading of the script, the trajectory of the LMC is calculated using the Orbit Calculator and the standard model with the Allen & Santillan-potential. Two trajectories are calculated each 5000 Myrs into the past and future and stored in the two arrays *lmcn.tr.o0* and *lmcp.tr.o0* for positive and negative time values.

Interpolation of LMC postions from the trajectory file

```
define lmc_inter(t){
    variable xlmc, ylmc, zlmc;
    if(t<0){
        xlmc = interpol(-t, -lmcn.tr.o0.t, lmcn.tr.o0.x);
        ylmc = interpol(-t, -lmcn.tr.o0.t, lmcn.tr.o0.y);
        zlmc = interpol(-t, -lmcn.tr.o0.t, lmcn.tr.o0.z);
    }else{
        xlmc = interpol(t, lmcp.tr.o0.t, lmcp.tr.o0.x);
        ylmc = interpol(t, lmcp.tr.o0.t, lmcp.tr.o0.y);
        zlmc = interpol(t, lmcp.tr.o0.t, lmcp.tr.o0.z);
    }
    return (xlmc,ylmc,zlmc);
}
```

As the differential equation solver adaptively determines the length of time steps to keep errors low, the time steps of later trajectory simulations generally do not match those of the LMC's trajectory. Thus a function is defined to determine the position of the LMC at any time. As argument, it takes any time value between -5000 and 5000 Myrs and returns the according coordinates *xlmc*, *ylmc*, *zlmc*. The values are interpolated linearly from the LMC trajectory arrays *lmcn.tr.o0* and *lmcp.tr.o0* using ISIS's *interpol()* function. The case distinction makes sure the correct array is used.

The following changes are part of the function *AS_LMC()* where the model potential's derivatives are stored seperately, to be called by the differential equation solver.

Additional constants

```
variable Mb = qualifier("Mb", 409.); % mass of the bulge
variable bb = qualifier("bb", 0.23); % scale length bulge
...
variable Mlmc = qualifier("Mlmc", 860.); % mass of LMC
variable blmc = qualifier("blmc", 1.0148); % scale length of LMC
```

To the above list of constants the Mass $Mlmc$ in Galactic mass units (see section 3) and scale length $blmc$ in kpc of the LMC potential are added.

Determine current LMC coordinates

```
variable xa, ya, za;
(xa, ya, za) = lmc_inter(t);
```

The interpolation function described above is called to determine the LMC position for the current time-step and store it in three variables.

Storing frequently appearing expressions

```
variable sin_ya = sin(phi)*r-ya;
variable cos_xa = cos(phi)*r-xa;

variable dPot_lmc =
    -Mlmc/(2*((z-za)^2+sin_ya^2+cos_xa^2+blmc^2)^(1.5));
```

Larger expressions that appear in all three dimensions of the Force equations are stored in their own variables to save runtime.

Calculating derivatives of the whole potential

```
variable dPotdr = constant*( dPot_bulge*r + dPot_disc*r +
    dPot_lmc*(2*sin(phi)*sin_ya+2*cos(phi)*cos_xa) );

variable dPotdz = constant*( dPot_bulge*z +
    dPot_disc*(ad+sz2bd2)/sz2bd2*z + dPot_lmc*2*(z-za) );

variable dPotdphi = constant*dPot_lmc*(2*cos(phi)*r*sin_ya -
    2*sin(phi)*r*cos_xa);
```

The two Potential derivatives of r and z get the additional terms described in 5.2. The expression for $dPotdphi$ is newly introduced, as before it was zero and thus not required.

Erklärung

Hiermit versichere ich, dass ich die vorliegende Arbeit selbstständig verfasst und keine anderen als die angegebenen Quellen und Hilfsmittel benutzt habe, dass alle Stellen der Arbeit, die wörtlich oder sinngemäß aus anderen Quellen übernommen wurden, als solche kenntlich gemacht sind und dass die Arbeit in gleicher oder ähnlicher Form noch keiner Prüfungsbehörde vorgelegt wurde.

Erlangen, den 14. Oktober 2013